ACS OMEGA

Open Access

http://pubs.acs.org/journal/acsodf

Article

Validating the Transition Criteria from the Cassie−Baxter to the Wenzel State for Periodically Pillared Surfaces with Lattice Boltzmann Simulations

Tobias Jäger,* Athanasios Mokos,* Nikolaos I. Prasianakis,* and Stephan Leyer*

Cite This: *ACS Omega* 2024, 9, 10592−10601

Read Online

ACCESS | Metrics & More | Article Recommendations

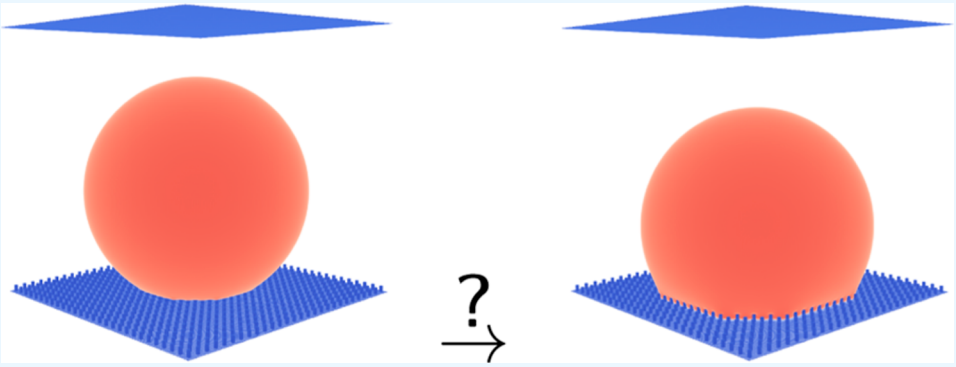

ABSTRACT: Microfabrication techniques allow the development and production of artificial superhydrophobic surfaces that possess a precisely controlled roughness at the micrometer level, typically achieved through the arrangement of micropillar structures in periodic patterns. In this work, we analyze the stability and energy barrier of droplets in the Cassie−Baxter (CB) state on such periodic patterns. In addition, we further develop a transition criterion using the CB equation and derive an improved version which allows predicting for which pillar geometries, equilibrium contact angles, and droplet volumes the CB state switches from a metastable to an unstable state. This enables a comparison with existing experiments and three-dimensional multiphase Lattice Boltzmann simulations for different pillar distances, two contact angles, and two droplet volumes, where a good agreement has been found.

INTRODUCTION

Superhydrophobic surfaces have garnered significant attention because of their outstanding wetting properties and various potential technological applications.[1] Their production has significantly advanced due to improved microfabrication techniques that allow for controlled local roughness at the micrometer scale. Often, these roughnesses are created by periodically arranged micropillar structures.[2−7] Among other applications, this is especially interesting for membrane distillation; Xiao et al.[7] showed that micropillars and hydrophobic coatings have the capability to decrease scaling and extend the operational duration of a membrane. While the development of artificial superhydrophobic surfaces has made progress, certain fundamental aspects regarding the wetting behavior of these surfaces still raise debate. One particular unresolved issue concerns the transition from the superhydrophobic state,[1] known as the Cassie−Baxter (CB) state,[8] for which gas is trapped within the surface roughness, to the completely wet state, known as the Wenzel (W) state.[9] During the transition, the apparent contact angle is decreased, and most of the desirable superhydrophobic characteristics of the surface are lost.[4,7]

It is generally accepted that for many common geometries, the CB state is metastable or unstable. If an energy barrier between the two states is overcome, the transition to the energetically stable Wenzel state occurs.[10−13] This energy barrier can already be overcome due to small perturbations such as surface waves created by gravitational or capillary forces at the liquid−air interface.[4] The transition behavior is often approached by describing the Gibbs free energy for the problem. Based on the function for Gibbs free energy, different transition criteria have been formulated.[3,6,10,12,14,15] An

Received: November 7, 2023
Revised: February 8, 2024
Accepted: February 12, 2024
Published: February 20, 2024

https://doi.org/10.1021/acsomega.3c08862
ACS Omega 2024, 9, 10592−10601

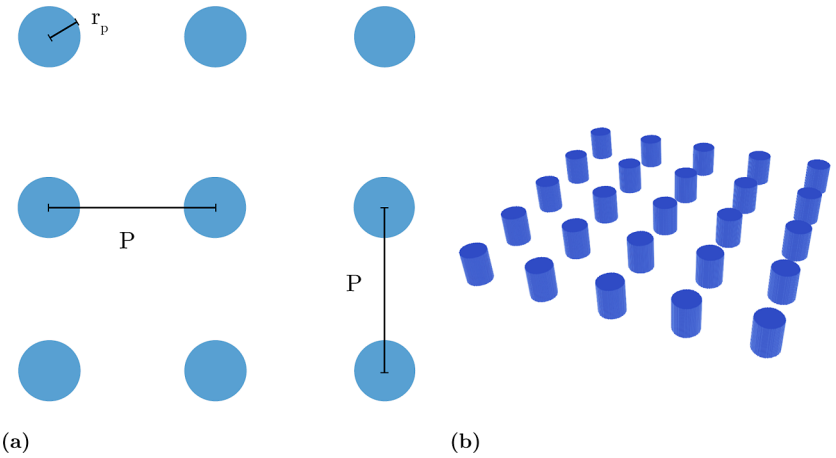

Figure 1. (a) Aerial view (reprinted with permission from Jäger et al.[16] CC BY 4.0) and (b) corresponding 3D structure of a periodically pillared surface with a quadratic unit cell and round pillars.

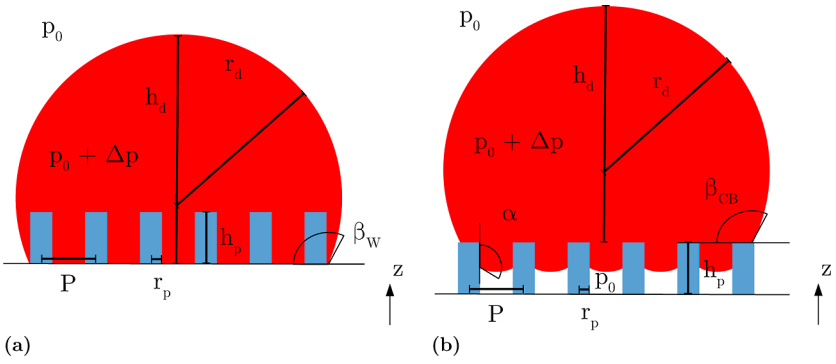

Figure 2. (a) Droplet in the Wenzel state and (b) droplet in an intermediate state. α is the contact angle between the liquid and the vertical pillar wall.

intermediate state, where the liquid wets the pillar walls but does not reach the bottom, also exists.[6]

Jung and Bhushan[4,5] observed in experiments that beyond certain pillar distances, droplets transition from the CB into the Wenzel state. Jäger et al.[16] compared Lattice Boltzmann (LB) simulations to the experimental study from Jung and Bhushan[4] and observed a qualitatively similar behavior for the transition from CB to Wenzel state but observed a much lower critical pillar distance. Zheng et al.[12] and Patankar[11] already developed a transition criterion based on a critical pressure difference and the Young−Laplace pressure difference. In this work, we try to answer the question of which quantities determine the critical pillar distance and aim to derive a formula that allows us to predict the critical pillar distance for a given droplet volume. This allows a comparison to experiments and simulations. In wetting experiments where a droplet is placed on a periodically pillared surface, one can often control the droplet volume; therefore, it is beneficial to know if and how the droplet volume affects the critical pillar distance.

Two mechanisms were identified for this transition: (a) Jung and Bhushan[4] argued that the transition occurs if the droop/sag (δ) at the bottom side of the droplet is much greater than the pillar height (h_p). (b) Patankar[11] derived a transition criterion based on the pressure differences: even before the droop touches the pillar bottom, the Young−Laplace pressure difference Δp between the inside of the liquid droplet and the surrounding air pressure p_0 can result in penetration of liquid between the pillars, ultimately leading to wetting of the bottom between the pillars. Murakami et al.[6] also observed that the Young−Laplace pressure difference is much greater than the hydrostatic pressure on the bottom side of the droplet because of gravity. For small droplets, this suggests that the Young−Laplace pressure difference is an important aspect for the transition from the CB to the Wenzel state. The two aforementioned transition mechanisms can both independently of each other lead to a transition from a CB to the Wenzel state.[11]

The paper is structured as follows: we first give a theoretical background to the problem, particularly regarding the work of Zheng et al.[12] and Patankar,[11] who derived a condition for the critical pressure for an arbitrary periodically pillared surface. We then give a brief overview of the LB multiphase model that is being used to characterize the stability of the CB state. We further develop the condition from Patankar[11] and Zheng[12] using the CB equation[8] and derive a condition which allows predicting for which pillar geometries, equilibrium contact angles, and droplet volumes the CB state switches from a metastable to an unstable state. This condition additionally allows comparison of the theoretical predictions to multiphase LB simulations and existing experiments for multiple pillar geometries.

THEORETICAL BACKGROUND

A periodically pillared surface is characterized by A, the cross-sectional area of the pillar, the rectangular unit cell area A_c which is repeated periodically in x- and y-directions, the pillar

https://doi.org/10.1021/acsomega.3c08862
ACS Omega 2024, 9, 10592−10601

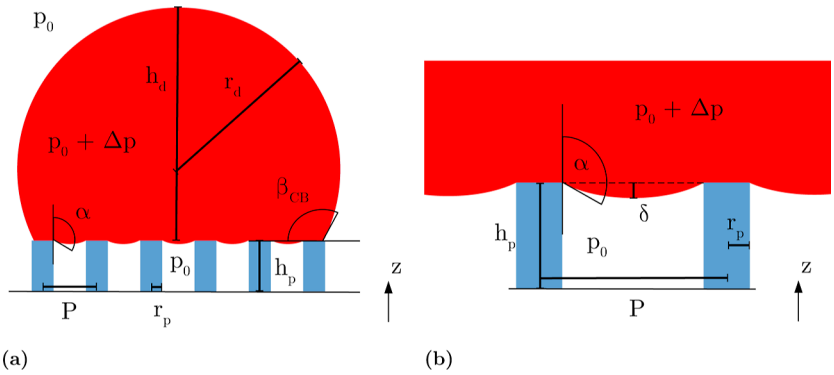

Figure 3. Droplet in the CB state. Full droplet in (a) and the droplet bottom in (b).

perimeter l, and the pillar heights h_p. For a quadratic unit cell with pillar distance P (see Figure 1), $A_c = P \times P$ holds. For pillars with a circular cross section, $l = 2\pi r_p$ and $A = \pi r_p^2$ and for pillars with quadratic cross section, $l = 4d_p$ and $A = d_p^2$ with pillar side length d_p.

Bond number (Bo) is a dimensionless quantity that characterizes the balance between gravitational and capillary forces[17] and is expressed through the subsequent equation: $\mathrm{Bo} = \Delta\rho g L^2/\gamma$, where g denotes the gravitational acceleration, $\Delta\rho$ is the difference in the density of liquid and gas, γ denotes the surface tension, and L represents the characteristic length. In the context of liquid droplets, the characteristic length L corresponds to the droplet radius. When the bond number is much smaller than 1 ($\mathrm{Bo} \ll 1$), gravitational effects can be considered negligible.

Wenzel and CB Equation. The equilibrium contact angle α_0 on a flat surface of the same material and the apparent contact angle β_W for a droplet in the Wenzel state (Figure 2) are connected through the Wenzel equation.[9] For details, see the Appendix.

In the case of a droplet in the CB state,[8] in contrast, the equilibrium contact angle α_0 for a similar surface is connected to the apparent contact angle β_{CB} through the subsequent equation

$$\cos\beta_{CB} = \frac{A}{A_c}(\cos\alpha_0 + 1) - 1 \tag{1}$$

If gravitation is negligible, the shape of a droplet in the CB state can be approximated by a spherical cap (see Figure 3), and the droplet radius r_d is given by

$$r_d = \sqrt[3]{\frac{3V_d}{\pi(2+\cos\beta_{CB})(1-\cos\beta_{CB})^2}} = \sqrt[3]{\frac{3V_d}{\pi\left(1+\frac{A}{A_c}(\cos\alpha_0+1)\right)\left(2-\frac{A}{A_c}(\cos\alpha_0+1)\right)}} \tag{2}$$

where V_d is the volume of the droplet (spherical cap). Equation 1 can be used to eliminate the apparent contact angle of the droplet β_{CB} in the equation for the droplet radius.

Stability of the CB and Wenzel States. Based on an equation for the Gibbs free energy by Patankar[10] (shown in the Appendix), Zheng[12] derived a condition to evaluate which of the two droplet states (CB or Wenzel) is the stable state

$$-\cos\beta_W < -\cos\beta_{CB} \tag{3}$$

If that is true, the Wenzel state is stable, whereas the CB wetting mode is meta stable or even unstable.[12,13] In this study, the emphasis is directed toward situations in which the Wenzel state is the stable state with the analysis focusing on which geometries the droplet in the CB state switches from a meta stable to an unstable state.

Young−Laplace Equation. According to Laplace,[18] the pressure difference across a liquid−gas interface Δp is linked to the mean curvature of the interface and the liquid surface tension γ. In a static scenario, where external forces such as gravity are negligible, the pressure difference at the interface is independent of the spatial location. Consequently, the pressure difference Δp is constant everywhere along the liquid−gas interface, including both the liquid−gas interface on top of the droplet and the one between the pillars.

If gravitation is negligible, a droplet in the CB state can be approximated by a spherical cap of radius r_d, and therefore one can calculate the pressure difference according to Laplace[18] by

$$\Delta p = \gamma\frac{2}{r_d} \tag{4}$$

Transition Criterion. *Critical Pressure and Energy Barrier for Periodically Pillared Surfaces.* Zheng et al.[12] used a force balance approach to derive a general expression to calculate the critical pressure for a liquid film on an arbitrary periodically pillared structure and found good agreement with numerical simulations. Jäger et al.[19] were able to confirm their results with multiphase LB simulations. In the critical state, according to[12]

$$F_z = \Delta p_{crit}(A_c - A) + \gamma l \underbrace{\cos(\alpha_0)}_{\substack{\text{projection}\\ \text{along}\\ z\text{-axis}}} = 0 \tag{5}$$

Rearranging gives[12]

$$\Delta p_{crit} = -\frac{\gamma l\cos(\alpha_0)}{A_c - A} \tag{6}$$

Patankar[11] concluded that the CB state transits to the Wenzel state if the Young−Laplace pressure difference ($\Delta p = 2\gamma/r_d$) exceeds the critical value Δp_{crit} (shown in eq 6) and showed that the same condition can be derived when considering the energy barrier and the work done when the liquid moves down the pillar.

If the pressure difference between the liquid above the pillars and the air below exceeds the critical pressure difference Δp_{crit}, the liquid starts to move down the pillars. Based on the work

https://doi.org/10.1021/acsomega.3c08862
ACS Omega 2024, 9, 10592−10601

needed to move down the liquid, Patankar[3] and Zheng[12] calculated the magnitude of the energy barrier per area from CB to Wenzel state by

$$\Gamma_{CB-W} = h_p \Delta p_{crit} \frac{A_c - A}{A_c} = -\frac{h_p \gamma l \cos(\alpha_0)}{A_c} \quad (7)$$

Sag Transition. Jäger et al.[4] and Patankar[11] estimated the droop/sag δ by a spherical approximation of the liquid gas interface and obtained $\delta = r_d - \sqrt{r_d^2 - (\sqrt{2}P - 2r_p)^2/4}$. Here, $\sqrt{2}P$ is the diagonal distance between two pillar centers, and r_p is the pillar radius. For quadratic pillars, the previous equation can be modified as

$$\delta = r_d - \sqrt{r_d^2 - (\sqrt{2}P - \sqrt{2}d_p)^2/4} \quad (8)$$

A transition to the Wenzel state occurs when $\delta \geq h_p$.[4,11] Patankar[11] concluded that the sag transition is likely to occur only when the Wenzel state leads to lower energy than the CB state.

NUMERICAL METHOD

To determine the interface of a droplet on top of a rough hydrophobic surface, this study uses a LB multiphase model with additional interactions between fluid and solid. This enables the adjustment of the equilibrium contact angle (α_0) between a flat solid surface and a liquid droplet and allows simulating the liquid−gas flow. Mesoscopic methods, like LB, provide viable predictions for intricate 3D structures, both on the micro- and nano-scales. These methods can be categorized into particle- and lattice-based approaches.[20] The LB framework shows promise due to its ability to handle complex boundary conditions, including rough surfaces.[21] Moreover, it is well-suited for parallelized calculations on GPUs,[20,22,23] enabling simulations in both the continuum and the slip flow regime.[24] In contrast to classical continuum based solvers, the fluid is described by a density distribution function $f(\mathbf{x}, \mathbf{v}, t)$ within the LB framework. $f(\mathbf{x}, \mathbf{v}, t)$ can be seen as an extension to the mass density, also containing information about the velocity distribution.

Similar to previous works, e.g.,[16,21] an isothermal multiphase LB method is employed in this study to predict the shape and state of liquid droplets on micropillar structures and to validate our theoretical findings. A D3Q27 lattice is used, which employs 27 discrete velocities ($\mathbf{c}_i$, i = 0....26) at every lattice node within a three-dimensional (3D) spatial framework.[25] During one time step of length Δt, the discrete distribution function $f_i(\mathbf{x}, t)$ is streamed to its neighboring nodes according to

$$f_i(\mathbf{x} + \mathbf{c}_i\Delta t, t + \Delta t) - f_i(\mathbf{x}, t) = -\frac{1}{\tau}[f_i(\mathbf{x}, t) - f_i^{eq}(\rho, \mathbf{v}, \mathbf{x}, t)] \quad (9)$$

Typically, the LB method uses the Bhatnagar−Gross−Krook approach to approximate the collisions between the fluid particles.[26] The viscosity is associated with relaxation time τ. Macroscopic quantities like velocity and density are derived by a summation over the discrete distribution function f_i and velocities c_i at a given point in space.[25] The LB method employs a dimensionless approach, where time step (Δt = 1 ts), lattice spacing (Δx = 1lu), and particle mass (m = 1 mu) are set to one unit each, providing stability and faster convergence as commonly done for LB simulations.[27] The method reproduces the Navier−Stokes equation in the hydrodynamic limit.[25]

$$\rho = \sum_{i=0}^{26} f_i \quad (10)$$

$$\mathbf{v} = \frac{1}{\rho}\sum_{i=0}^{26} f_i \mathbf{c}_i \quad (11)$$

In this study, the guided equilibrium model[25,28] was employed to calculate the equilibrium distribution f_i^{eq}. Additional implementation details are given in refs 16, 25, and 28. The selected multiphase model for this research was the Shan−Chen model,[27,29,30] which incorporates a pseudo potential to account for the interactions between fluid particles

$$\mathbf{F} = -G\psi(\mathbf{x}, t)\sum_{i=0}^{26} w_i\psi(\mathbf{x} + \mathbf{c}_i\Delta t, t)\mathbf{c}_i \quad (12)$$

G represents the fluid−fluid interaction strength and controls the surface tension of the fluid. The fluid−solid interaction is modeled by including an additional interaction force $\mathbf{F}_{ads}$, where $s(\mathbf{x})$ is a step function that takes the value 0 for fluid voxels and 1 for solid voxels.[27,31]

$$\mathbf{F}_{ads} = -G_{ads}\psi(\mathbf{x}, t)\sum_{i=0}^{26} w_i s(\mathbf{x} + \mathbf{c}_i\Delta t, t)\mathbf{c}_i \quad (13)$$

The model parameter G_{ads} exhibits a linear correlation with the equilibrium contact angle α_0 measured on a flat solid surface, as demonstrated in a benchmark presented in ref 16 Therefore, this enables the manipulation of the hydrophobicity by adjusting G_{ads}. Detailed information is given in refs 16, 27, and 29.

Furthermore, a nonslip boundary condition (achieved by a bounce-back of the distribution function) was utilized between the fluid and solid surfaces. Unless specified otherwise, periodic boundary conditions were applied in all directions at the boundaries of the computational domain.

For all LB simulations conducted here, we employed G = 120.0, which leads to a surface tension of γ = 14.04 mu ts^{-2} in LB units. This results in ρ_l = 524.4 mu lu lu^{-3} (liquid density) and ρ_g = 85.7 mu lu^{-3} (gas density) for a flat interface. To realize an equilibrium contact angle of 100°, we used G_{ads} = −174.52.

As the liquid−gas interface shape is solely influenced by the contact line of liquid gas and solid and the parameter $q := \Delta p/\gamma$ [lu^{-1}], it is enough to make sure that q corresponds to the physical problem to capture the correct interface shape. To dimensionalize the problem, the following relationship is used: $\Delta p^{SI}/\gamma^{SI} = q^{SI} = q/\Delta x^{SI}$, where Δx^{SI} represents the distance between two lattice nodes in SI units. As a consequence, for a droplet on top of the pillar structure, the interface shape is only determined by the droplet radius, the geometry of the pillars, and the equilibrium contact angle α_0. Equation 14 shows the convergence criterion for all simulations conducted in this work, fulfilled with $\varepsilon = 1 \times 10^{-6}$.

$$\varepsilon > \max_{x,y,z}\left(\frac{|\rho^t(x, y, z) - \rho^{t-1}(x, y, z)|}{\rho^{t-1}(x, y, z)}\right) \quad (14)$$

https://doi.org/10.1021/acsomega.3c08862
ACS Omega 2024, 9, 10592−10601

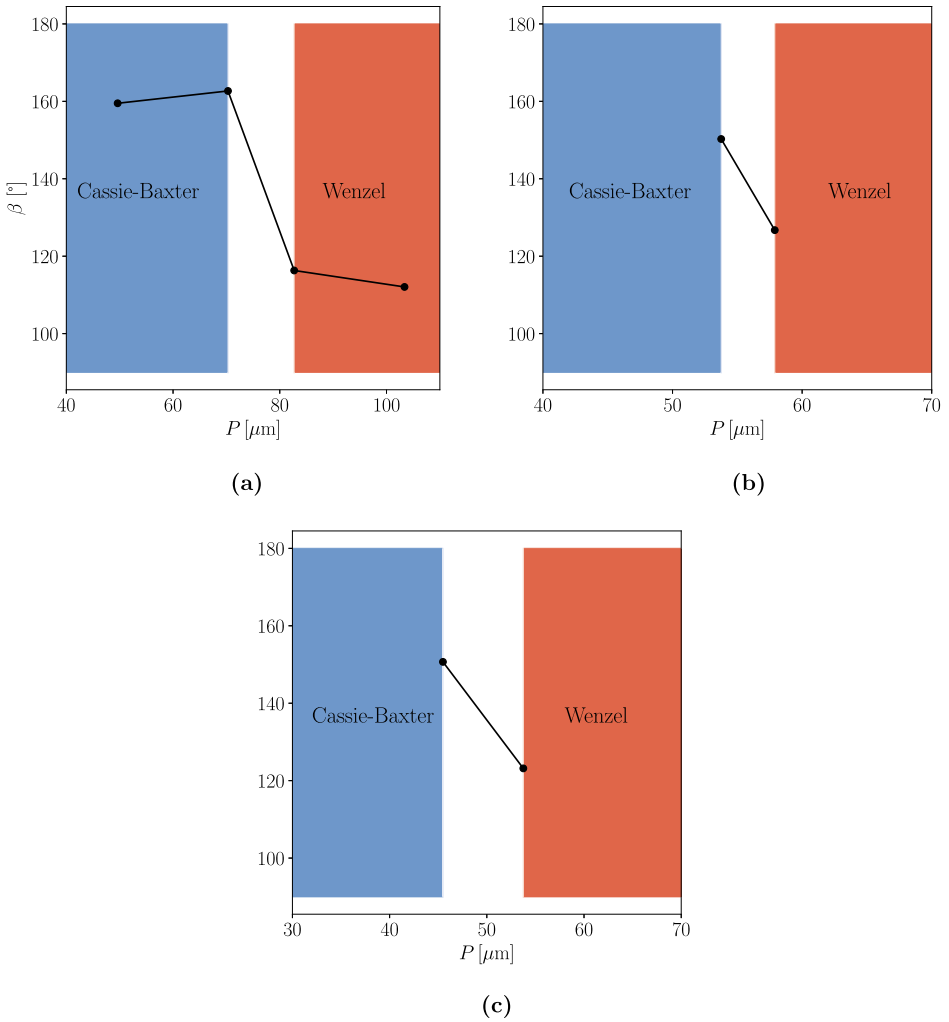

Figure 4. Multiphase simulation results LB1 (Adapted with permission from Jäger et al.[16] CC BY 4.0) in (a). Multiphase simulation results LB2 in (b) and LB3 in (c). The apparent contact angle β for the CB or Wenzel state as a function of the pillar distance P. The blue area marks the CB regime and the red area the Wenzel regime.

All simulations were conducted using an adapted high-performance computing code from Safi.[32] All 3D plots presented in this study were generated using ParaView[33]

RESULTS AND DISCUSSION

Energy Barrier and Transition Criterion for a Finite Droplet. If one places a finite droplet on top of a periodically pillared surface, the Young−Laplace pressure difference effectively lowers the energy barrier per area between the CB and Wenzel states, and a lower external pressure needs to be applied to achieve the transition. Therefore, based on the results from Patankar[11] and Zheng,[12] we propose a modified equation to calculate the energy barrier per area for droplets on periodically pillared surfaces

$$\Gamma_{\mathrm{CB-W,d}} = h_{\mathrm{p}}\left(\Delta p_{\mathrm{crit}} - 2\frac{\gamma}{r_{\mathrm{d}}}\right)\frac{A_{\mathrm{c}} - A}{A_{\mathrm{c}}} \tag{15}$$

Compared to eq 7, which is only applicable if the Young−Laplace pressure difference can be neglected, e.g., for a film on an infinite periodically pillared surface, the new eq 15 takes into account the curvature and is therefore applicable for a finite droplet. Equation 6 was similarly derived for a film on an infinite periodically pillared surface but still remains applicable if the droplet is in contact with multiple pillars. Therefore, it is still used for the calculation of Δp_{crit}. However, a droplet only in contact with a single pillar in the absence of gravity will always remain in a stable state; therefore, eq 6 is not applicable in this case.

It is crucial to keep in mind that this is only valid in the case where gravitation can be neglected, since in this case the pressure difference at the droplet interface does not depend on the direction and the droplet has the shape of a spherical cap with a radius r_{d}. As the bond number approaches 1, the assumption of a spherical cap is no longer reasonable. And an additional term accounting for gravity would enter the equation for the energy barrier and further lower the magnitude of the barrier.

Therefore, we can conclude that in the absence of gravity the energy barrier for a droplet depends not only on h_{p}, γ, l, A, A_{c}, and α_0 but also on r_{d}, the radius of the droplet. The smaller the droplet becomes, the lower the barrier gets. According to the criterion from Patankar[11] ($\Delta p > \Delta p_{\mathrm{crit}}$), an increase of the pressure difference, $\Delta p = 2\gamma/r$, increases the angle α (see Figure 3) until α_0 is reached and eq 4 equals eq 6. When this critical point is reached, the energy barrier vanishes completely, and the CB state switches from a metastable to an unstable

https://doi.org/10.1021/acsomega.3c08862
ACS Omega 2024, 9, 10592−10601

state. From this, one can derive a condition for the critical radius of the droplet

$$r_{\mathrm{d,crit}} = -2\frac{A_c - A}{l\cos(\alpha_0)} \tag{16}$$

It immediately becomes clear that when gravity is absent, the condition for the critical droplet radius in eq 16 is independent of the surface tension.

In experiments, one can often control the volume of the droplet. Therefore, we chose to use the relation for the droplet volume and the droplet (spherical cap) radius in eq 2 to reformulate eq 16.

$$V_{\mathrm{d,crit}}(l, A_c, A, \alpha_0, \beta_{\mathrm{CB}}) = -\frac{8\pi(A_c - A)^3(2 + \cos\beta_{\mathrm{CB}})(1 - \cos(\beta_{\mathrm{CB}}))^2}{3l^3\cos^3(\alpha_0)} \tag{17}$$

Using the CB (1 we can eliminate the apparent contact angle β_{CB}. With $A_c = P \times P$ for a quadratic periodically pillared surface, we then gain a condition (eq 18) for the critical volume which only depends on l the perimeter of the pillar, P the distance between two pillars, A the top area of the pillars, and the equilibrium contact angle α_0.

$$V_{\mathrm{d,crit}}(l, P, A, \alpha_0) = -\frac{8\pi(P^2 - A)^3\left(1 + \frac{A}{P^2}(\cos\alpha_0 + 1)\right)\left(2 - \frac{A}{P^2}(\cos\alpha_0 + 1)\right)^2}{3l^3\cos^3(\alpha_0)} \tag{18}$$

Iterative root-finding procedures can be used to solve eq 18 numerically for the other variables (l, P, A, α_0). We used this procedure to calculate $P_{\mathrm{crit}}(\alpha_0, l, A, V)$ numerically and compare the predictions of condition 18 to experimental results from Jung and Bhushan[4] and multiphase LB simulations from Jäger et al.[16] (see Figure 4a) and new multiphase LB simulations for additional geometries (see Figure 4b,c). In Jung and Bhushan's[4] experiments, a droplet of 5 μL was placed on a periodically pillared surface; then they observed whether the static droplet ended up in either the CB or Wenzel state and measured the apparent contact angle. The experiment was repeated for different pillar distances P. Therefore, Jung and Bhushan[4] were able to determine a range of P for which a transition from CB to Wenzel state takes place.

Numerical and Experimental Validation. Previously, Jäger et al.[16] compared the results from Jung and Bhushan[4] (Exp. 1 and 2) to multiphase LB simulations (LB1) with a similar geometry and equilibrium contact angle but a smaller droplet of only 1 μL volume due to computational limitations. Simulation results from Jäger et al.[16] (LB1) are shown in Figure 4 (a). They observed the same qualitative behavior in the simulations, but the transition from CB to Wenzel state occurred for a smaller P compared to the experimental study by Jung and Bhushan[4] (see Table 1). We also added the theoretical predictions for P_{crit} based on eq 18 in Table 1.

In the LB simulations, the droplet transitions to a different state even in the absence of gravity and with zero initial velocity because, after initializing a spherical droplet just above the pillar structure, small oscillations occur until the liquid and gas density converged to their equilibrium values. This is enough perturbation to make the transition happen if the critical state is reached. These dampened oscillations are typical for LB multiphase simulations and vanish over time.

Table 1. Observed and Theoretically Predicted Critical Pillar Distance P_{crit} for Different Experimental and Numerical (LB1, LB2, LB3) Setups

	Exp. 1 Jung[4]	Exp. 2 Jung[4]	LB1[16]	LB2	LB3
α_0 [°]	109	109	109	100	100
l [μm]	15.708	43.982	49.62	66.16	49.62
A [μm^2]	19.635	153.938	153.88	273.57	153.88
V_{d} [μL]	5	5	1	1	1
h_{p} [μm]	10	30	33.08	33.08	33.08
stable state	Wenzel	Wenzel	Wenzel	Wenzel	Wenzel
δ [μm]	2	4	5	3	2
Bo	0.24	0.24	0.083	0.083	0.082
observed P_{crit} [μm]	44−60	125−167	70−83	54−58	45−54
[lu]			17−20	13−14	11−13
predicted P_{crit} [μm]	52.27	88.03	71.87	61.96	53.17

In this paper, we investigate two additional pillar geometries (LB2 and LB3) with the same multiphase LB method. The corresponding results for the droplet state and the contact angle are shown in Figure 4b,c. An example of a droplet in the CB or the Wenzel state is given in Figure 5. For all LB simulations in this paper, we used rectangular pillars of either $A = 3 \times 3$ lu^3 or $A = 4 \times 4$ lu^3. Here, $\Delta x = 1$ lu $\equiv 4.135$ μm was chosen to match the geometries in the experimental study from Jung and Bhushan.[4] A spherical droplet of volume 1 μL is initialized right above the pillar structure with zero velocity according to eq 19

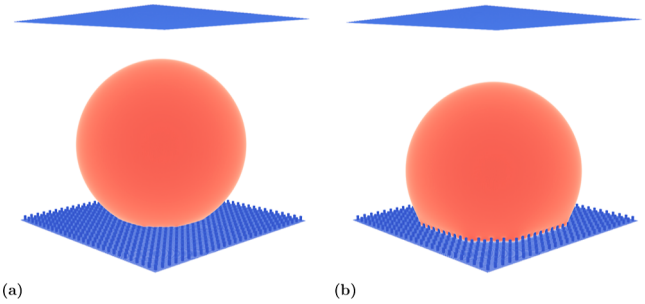

Figure 5. Droplet in contact with geometry LB2. In (a) is shown a droplet in the CB state for $P = 54$ μm and in (b) is shown a droplet in the Wenzel state $P = 58$ μm.

$$\rho(x, y, z) = \frac{\rho_l + \rho_g}{2} + \frac{\rho_g - \rho_l}{2} \times \tanh\left(\frac{2[\sqrt{(x - x_0)^2 + (y - y_0) + (z - z_0)^2} - r]}{5}\right) \tag{19}$$

for every simulation with $r = 150$lu. This leads to a volume of $V_{\mathrm{d}} \approx 1.0$ μL.

Total domain size was about $370 \times 370 \times 370$ lu$^3 \equiv 3.58$ mm^3 for each simulation. For all the setups which we investigated numerically, we ensured full contact with the droplet in the Wenzel state for at least 9 pillars.

In Figure 6 the dependence of the critical volume on the pillar distance P according to eq 18 is shown for the two experiments and the LB simulations. The intersection of $V_{\mathrm{d,crit}}(P)$ with a given droplet volume V_{d} gives a predicted value

https://doi.org/10.1021/acsomega.3c08862
ACS Omega 2024, 9, 10592−10601

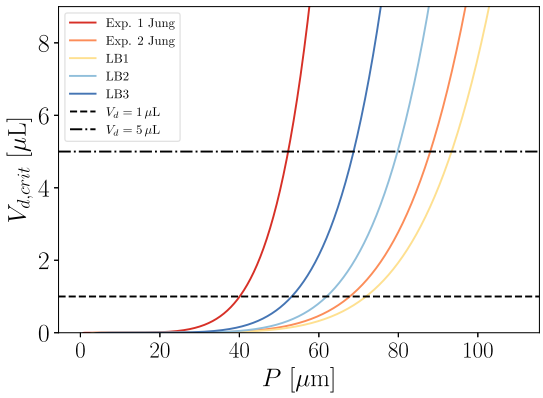

Figure 6. Dependence of the critical droplet volume $V_{d,crit}$ on the pillar distance P according to eq 18 for different experimental[4] and numerical (LB1,[16] LB2, LB3) setups.

for P_{crit}. Table 1 contains the experimental and simulation parameters (experiment 1, experiment 2, and LB simulations LB1, LB2, and LB3), as well as the observed and theoretically predicted values for P_{crit}. For all analyzed geometries, according to eq 3 the Wenzel state is the stable configuration, and since the sag is much smaller than the pillar heights ($\delta < h_p$) the transition occurs due to the Young−Laplace pressure difference (see Table 1). The bond number was calculated to be below 1 for all droplets.

Comparing these results with the two experiments by Jung and Bhushan[4] and LB simulations (see Table 1), we found very good agreement for experiment 1 and the LB simulations; the predicted critical values P_{crit} based on condition 18 lie within the observed range; only for LB simulation 2 the predicted value was slightly high. For the setup from experiment 2, the predicted value (P_{crit} = 88.03 μm) is below the range (125−167 μm) found in the experiment by Jung and Bhushan.[4] Figure 7b,d show the Wenzel and CB states for LB2, respectively.

We also simulated cases with equilibrium contact angles larger than 109°. However, this results in a state in which the droplet is in contact with only a few pillars. Therefore, these results are not comparable to the theoretical transition criterion.

It is important to mention that for the present LB simulations, a change in the pillar height can also change the droplet state. For example, for the LB2 setup, if we increase the pillar height to h_p = 49.62 μm and rerun the simulations, no transition to the Wenzel state was observed for P = 58 μm (see Figure 7a). Whereas for pillars with a height h_p = 33.08 μm, as reported in Table 1, we observed a transition to the Wenzel state for P = 58 μm (see Figure 7b). Increasing P for h_p = 49.62 μm, we can also observe a transition to the intermediate state (see Figure 7c).

To compare the influences of the different variables on the critical droplet volume $V_{d,crit}$, we calculated the partial derivatives of $V_{d,crit}$ in eq 18 with respect to the variables A, l, P, and α_0 and listed the magnitude of the derivatives in Table 2.

$$\frac{\partial V_{d,crit}}{\partial A} = \frac{8(-A + P^2)^2\pi(A - 2P^2 + A\cos(\alpha_0))(2(A^2 - AP^2 - P^4) + A(4A - 3P^2)\cos(\alpha_0) + A(2A - P^2)\cos^2(\alpha_0))}{l^3P^6\cos^3(\alpha_0)} \quad (20)$$

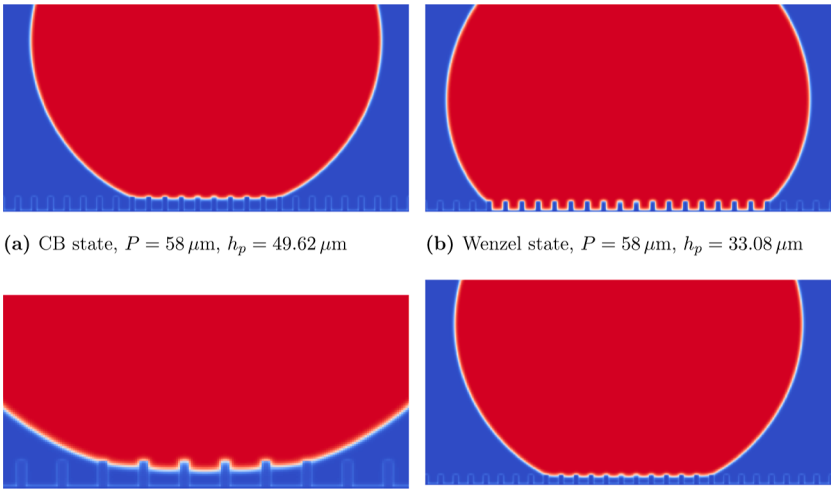

(a) CB state, $P = 58\,\mu$m, $h_p = 49.62\,\mu$m

(b) Wenzel state, $P = 58\,\mu$m, $h_p = 33.08\,\mu$m

(c) Intermediate state, $P = 79\,\mu$m, $h_p = 49.62\,\mu$m

(d) CB state, $P = 54\,\mu$m, $h_p = 33.08\,\mu$m

Figure 7. Slice of a 3D droplet (in red) on a periodically pillared surface from the present LB simulation results. For all setups shown in this figure, $A = 4 \times 4$ lu^3 holds, $\alpha_0 = 100°$.

https://doi.org/10.1021/acsomega.3c08862
ACS Omega 2024, 9, 10592−10601

Table 2. Influence of the Different Variables on $V_{d,crit}$

$\frac{1}{V_{crit}}\frac{\partial V_{d,crit}}{\partial A}$	$\frac{1}{V_{crit}}\frac{\partial V_{d,crit}}{\partial l}$	$\frac{1}{V_{crit}}\frac{\partial V_{d,crit}}{\partial P}$	$\frac{1}{V_{crit}}\frac{\partial V_{d,crit}}{\partial \alpha_0}$	A	l	P	α_0	V_{crit}
[μm^{-2}]	[μm^{-1}]	[μm^{-1}]	[1/°]	[μm^2]	[μm]	[μm]	[deg]	[μL]
−0.00020	−0.03431	0.02077	−0.76282	19.63	15.71	52.27	109	5
−0.000071	−0.01225	0.01249	−0.76285	153.94	43.98	88.03	109	5
−0.00011	−0.01086	0.01546	−0.76288	153.88	49.62	71.87	109	1

$$\frac{\partial V_{d,crit}}{\partial l} = -\frac{8(A - P^2)^3\pi(A - 2P^2 + A\cos(\alpha_0))^2(A + P^2 + A\cos(\alpha_0))}{l^4P^6\cos^3(\alpha_0)} \tag{21}$$

$$\frac{\partial V_{d,crit}}{\partial P} = -\frac{16(-A + P^2)^2\pi(A - 2P^2 + A\cos(\alpha_0))(A^3 - AP^4 - 2P^6 + (2A^3 - AP^4)\cos(\alpha_0) + A^3\cos^2(\alpha_0))}{l^3P^7\cos^3(\alpha_0)} \tag{22}$$

$$\frac{\partial V_{d,crit}}{\partial \alpha_0} = \frac{8(A - P^2)^3\pi(A - 2P^2 + A\cos(\alpha_0))(A^2 - AP^2 - 2P^4 + A(A - P^2)\cos(\alpha_0))\tan(\alpha_0)}{l^3P^6\cos^3(\alpha_0)} \tag{23}$$

As shown in Table 2, we found that the equilibrium contact angle has by far the largest influence among all of the parameters. A 3° higher equilibrium contact angle for experiment 2 (α_0 = 112°) leads to a predicted P_{crit} = 94.3 μm. Therefore, an error in the equilibrium contact angle measurements alone can not explain the difference between observation and theoretical prediction for experiment 2, but it can explain the small difference observed in the LB2 simulations (see Table 1). A possible explanation is that in experiment 2 the droplet switched and maintained the intermediate state instead of fully transitioning to the Wenzel state when reaching P_{crit}. This hypothesis is supported by the equation for the energy barrier (eq 15), which increases linearly with h_p. Experiments 1 and 2 have the same droplet volume, but the pillar heights differ by a factor of 3, which could explain the difference in predictions between experiments 1 and 2.

We also observed in the LB simulations that the transition to the Wenzel state depends on h_p. Even if the energy barrier in eq 15 completely vanished when P_{crit} is reached, one still needs some perturbation to make the transition to the Wenzel state happen. In the absence of gravity, as for our simulation, the oscillation of the droplet after the initialization provides the perturbation needed to make the transition happen. If the pillars are too high the perturbations dampen out before the transition to the Wenzel state is completed, and the droplet remains in the Wenzel or intermediate state. During the transition and especially for high pillars, the droplet radius and therefore the Young−Laplace pressure difference could decrease and the critical pressure might not be reached anymore, and the droplet gets stuck in the intermediate state.

CONCLUSIONS

Based on the work of Patankar[11] and Zheng et al.,[12] we have derived an equation for the energy barrier between CB and Wenzel states for droplets on periodically pillared surfaces. Due to the curvature of the droplets, there is a pressure difference between the droplet and the surrounding air, which lowers the transition barrier from the CB to the Wenzel state. The smaller the droplet becomes, the lower the transition barrier becomes. Furthermore, we derived a condition which allows to calculate the pillar geometries, equilibrium contact angles, and droplet volumes for which the CB state becomes unstable, which is especially useful if one wants to compare the theoretical findings from Patankar[11] and Zheng[12] to experimental results or simulations. The criterion in eq 16 is applicable for droplets on any periodically arranged roughness with vertical lateral surfaces and a flat horizontal top surface if gravitation is negligible and the area of the unit cell A_c is much smaller than the droplet cross section.

Based on theoretical considerations, we can conclude that the droplet size has a significant effect on the stability of the CB state. The surface tension plays a role only in the magnitude of the energy barrier. These findings are validated with experimental results and 3D multiphase LB simulations for two equilibrium contact angles (100 and 109°) and two droplet volumes (1 and 5 μL). The emphasis of this work was on the influence of pillar spacing, for which we found good agreement. To further validate the predictive power of 18 more experiments and LB simulations for different droplet volumes and different equilibrium contact angles are needed.

APPENDIX

Wenzel equation

The Wenzel equation[9] links the apparent contact angle in the Wenzel state to the equilibrium contact angle α_0.

$$\cos\beta_W = R_f\cos\alpha_0 \tag{24}$$

Here, R_f is the roughness factor defined by the ratio of rough to planar surface areas. For periodically repeated pillars, $R_f = 1 + A_l/A_c$, where $A_l = l \times h_p$ is the lateral surface of the pillar.

https://doi.org/10.1021/acsomega.3c08862
ACS Omega 2024, 9, 10592−10601

Gibbs Free Energy for a Droplet

Patankar[10] derived an equation for the Gibbs free energy E_G of a droplet with the shape of a spherical cap in contact with the pillar structure in any state.

$$E_G = (9\pi)^{1/3} V_d^{2/3} \gamma (2 - 3\cos(\beta) + \cos^3(\beta))^{1/3} \quad (25)$$

Since E_G is a strictly monotonically increasing function of $-\cos(\beta)$ in eq 25, the following relation needs to be true for the Wenzel wetting mode to be associated to a lower Gibbs free energy than the CB:[3,10,12,13] $-\cos\beta_W < -\cos\beta_{CB}$

AUTHOR INFORMATION

Corresponding Authors

Tobias Jäger − *Department of Engineering, Faculty of Science, Technology and Medicine, University of Luxembourg, Luxembourg L-1359, Luxembourg*; orcid.org/0000-0002-6588-2417; Email: tobias.jaeger@uni.lu

Athanasios Mokos − *Transport Mechanisms Group, Laboratory for Waste Management, Paul Scherrer Institute, Villigen 5232, Switzerland*; Email: athanasios.mokos@psi.ch

Nikolaos I. Prasianakis − *Transport Mechanisms Group, Laboratory for Waste Management, Paul Scherrer Institute, Villigen 5232, Switzerland*; Email: nikolaos.prasianakis@psi.ch

Stephan Leyer − *Department of Engineering, Faculty of Science, Technology and Medicine, University of Luxembourg, Luxembourg L-1359, Luxembourg*; Email: stephan.leyer@uni.lu

Complete contact information is available at: https://pubs.acs.org/10.1021/acsomega.3c08862

Author Contributions

Conceptualization, T. Jäger; methodology, T. Jäger, N. I. Prasianakis, and S. Leyer; software, T. Jäger, A. Mokos, N.I. Prasianakis; validation, T. Jäger, A. Mokos, N. I. Prasianakis, and S. Leyer; formal analysis, T. Jäger; investigation, T. Jäger, A. Mokos, N. I. Prasianakis, and S. Leyer; resources, N. I. Prasianakis and S. Leyer; data curation, T. Jäger; writing−original draft preparation, T. Jäger ; writing−review and editing, T. Jäger, A. Mokos, N. I. Prasianakis, and S. Leyer; visualization, T. Jäger; supervision, A. Mokos, N. I. Prasianakis, and S. Leyer; project administration, T. Jäger, N. I. Prasianakis, and S. Leyer; funding acquisition, N. I. Prasianakis and S. Leyer. All authors have read and agreed to the published version of the manuscript.

Funding

University of Luxembourg, Paul Scherrer Institute. This research received no external funding.

Notes

The authors declare no competing financial interest.

ACKNOWLEDGMENTS

The calculations in this paper were carried out using the HPC facilities of the University of Luxembourg[34] (see `hpc.uni.lu`) and the Swiss Supercomputing Center CSCS (project s1155). We also thank the University of Luxembourg and SwissNuclear for its support.

NOMENCLATURE

Δp_{crit}	critical pressure difference
γ	surface tension
q	$\Delta p/\gamma$
r_p	pillar radius
α	contact angles between the liquid and the pillar wall
α_0	equilibrium contact angle between liquid and solid
P	pillar distance (periodicity in x- and y-directions)
A_c	area of the periodically repeated cell ($A_c = P \times P$)
A	top area of the pillar
l	perimeter of the pillar
LB	lattice Boltzmann
p	pressure
ρ	density
ρ_l	liquid density
ρ_g	gas density
$\mathbf{F}$	force
Δx	lattice spacing
Δt	time step
m	fluid particle mass
G_{ads}	LB parameter to tune the equilibrium contact angle
G	LB parameter to control the fluid−fluid interaction strength
τ	relaxation time
ν	kinematic viscosity
c_s	speed of sound
g	gravitation acceleration
$\mathbf{v}$	velocity
$\mathbf{c}_i$	discrete lattice velocity

REFERENCES

(1) Giacomello, A.; Chinappi, M.; Meloni, S.; Casciola, C. M. Metastable Wetting on Superhydrophobic Surfaces: Continuum and Atomistic Views of the Cassie-Baxter−Wenzel Transition. *Phys. Rev. Lett.* **2012**, *109*, 226102.

(2) Yoshimitsu, Z.; Nakajima, A.; Watanabe, T.; Hashimoto, K. Effects of Surface Structure on the Hydrophobicity and Sliding Behavior of Water Droplets. *Langmuir* **2002**, *18*, 5818−5822.

(3) Patankar, N. A. *Transition between Superhydrophobic States on Rough Surfaces*, 2004.

(4) Jung, Y.; Bhushan, B. Wetting behaviour during evaporation and condensation of water microdroplets on superhydrophobic patterned surfaces. *J. Microsc.* **2008**, *229*, 127−140.

(5) Bhushan, B.; Chae Jung, Y. Wetting study of patterned surfaces for superhydrophobicity. *Ultramicroscopy* **2007**, *107*, 1033−1041.

(6) Murakami, D.; Jinnai, H.; Takahara, A. Wetting Transition from the Cassie−Baxter State to the Wenzel State on Textured Polymer Surfaces. *Langmuir* **2014**, *30*, 2061−2067. PMID: 24494786

(7) Xiao, Z.; Zheng, R.; Liu, Y.; He, H.; Yuan, X.; Ji, Y.; Li, D.; Yin, H.; Zhang, Y.; Li, X.-M.; He, T. Slippery for scaling resistance in membrane distillation: A novel porous micropillared superhydrophobic surface. *Water Res.* **2019**, *155*, 152−161.

(8) Cassie, A. B. D.; Baxter, S. Wettability of porous surfaces. *Trans. Faraday Soc.* **1944**, *40*, 546−551.

(9) Wenzel, R. N. RESISTANCE OF SOLID SURFACES TO WETTING BY WATER. *Ind. Eng. Chem.* **1936**, *28*, 988−994.

(10) Patankar, N. A. On the Modeling of Hydrophobic Contact Angles on Rough Surfaces. *Langmuir* **2003**, *19*, 1249−1253.

(11) Patankar, N. A. Consolidation of Hydrophobic Transition Criteria by Using an Approximate Energy Minimization Approach. *Langmuir* **2010**, *26*, 8941−8945 PMID: 20158175.

(12) Zheng, Q.-S.; Yu, Y.; Zhao, Z.-H. Effects of hydraulic pressure on the stability and transition of wetting modes of superhydrophobic surfaces. *Langmuir* **2005**, *21*, 12207−12212.

(13) Yeo, J.; Choi, M. J.; Kim, D. S. Robust hydrophobic surfaces with various micropillar arrays. *J. Micromech. Microeng.* **2010**, *20*, 025028.

(14) Xue, Y.; Chu, S.; Lv, P.; Duan, H. Importance of Hierarchical Structures in Wetting Stability on Submersed Superhydrophobic Surfaces. *Langmuir* **2012**, *28*, 9440−9450.
(15) Lv, P.; Xue, Y.; Shi, Y.; Lin, H.; Duan, H. Metastable States and Wetting Transition of Submerged Superhydrophobic Structures. *Phys. Rev. Lett.* **2014**, *112*, 196101.
(16) Jäger, T.; Mokos, A.; Prasianakis, N. I.; Leyer, S. Pore-Level Multiphase Simulations of Realistic Distillation Membranes for Water Desalination. *Membranes* **2022**, *12*, 1112.
(17) Kunes, J. *Dimensionless Physical Quantities in Science and Engineering*; Elsevier Scientific Pub. Co Amsterdam: New York, 2012.
(18) de Laplace, P. S. *Supplément au dixième livre du Traité de Mécanique Céleste*; J.B.M. Duprat, 1805; Vol. *4*, pp 1−79.
(19) Jäger, T.; Keup, J.; Prasianakis, N. I.; Leyer, S. Theoretical and Numerical Constant Mean Curvature Surface and Liquid Entry Pressure Calculations for a Combined Pillar-Pore Structure. *Coatings* **2023**, *13*, 865.
(20) Schiller, U. D.; Krüger, T.; Henrich, O. Mesoscopic modelling and simulation of soft matter. *Soft Matter* **2018**, *14*, 9−26.
(21) Xiong, W.; Cheng, P. Mesoscale simulation of a molten droplet impacting and solidifying on a cold rough substrate. *Int. Commun. Heat Mass Tran.* **2018**, *98*, 248−257.
(22) Prasianakis, N. I.; Rosén, T.; Kang, J.; Eller, J.; Mantzaras, J.; Büichi, F. N. Simulation of 3D Porous Media Flows with Application to Polymer Electrolyte Fuel Cells. *Commun. Comput. Phys.* **2013**, *13*, 851−866.
(23) Rosen, T.; Eller, J.; Kang, J.; Prasianakis, N. I.; Mantzaras, J.; Büchi, F. N. Saturation dependent effective transport properties of PEFC gas diffusion layers. *J. Electrochem. Soc.* **2012**, *159*, F536−F544.
(24) Luo, K.; Xia, J.; Monaco, E. Multiscale modelling of multiphase flow with complex interactions. *J. Multiscale Model.* **2009**, *01*, 125−156.
(25) Prasianakis, N. I.; Karlin, I. V.; Mantzaras, J.; Boulouchos, K. B. Lattice Boltzmann method with restored Galilean invariance. In *Computational methods in fluid dynamics*; Kinetic theory, 2009.
(26) Qian, Y. H.; D'Humières, D.; Lallemand, P. Lattice BGK Models for Navier-Stokes Equation. *Europhys. Lett.* **1992**, *17*, 479−484.
(27) Peng, C.; Tian, S.; Li, G.; Sukop, M. C. Single-component multiphase lattice Boltzmann simulation of free bubble and crevice heterogeneous cavitation nucleation. *Phys. Rev. E* **2018**, *98*, 023305.
(28) Safi, M. A.; Mantzaras, J.; Prasianakis, N. I.; Lamibrac, A.; Büchi, F. N. A pore-level direct numerical investigation of water evaporation characteristics under air and hydrogen in the gas diffusion layers of polymer electrolyte fuel cells. *Int. J. Heat Mass Transfer* **2019**, *129*, 1250−1262.
(29) Shan, X.; Chen, H. Lattice Boltzmann model for simulating flows with multiple phases and components. *Phys. Rev. E* **1993**, *47*, 1815−1819.
(30) Shan, X.; Chen, H. Simulation of nonideal gases and liquid-gas phase transitions by the lattice Boltzmann equation. *Phys. Rev. E: Stat. Phys., Plasmas, Fluids, Relat. Interdiscip. Top.* **1994**, *49*, 2941−2948.
(31) Sukop, M. C.; Thorne, D. T. *Lattice Boltzmann Modeling*; Springer Berlin: Heidelberg, Germany, 2006.
(32) Safi, M. A.; Prasianakis, N. I.; Mantzaras, J.; Lamibrac, A.; Büchi, F. N. Experimental and pore-level numerical investigation of water evaporation in gas diffusion layers of polymer electrolyte fuel cells. *Int. J. Heat Mass Transfer* **2017**, *115*, 238−249.
(33) Ahrens, J.; Geveci, B.; Law, C. *Visualization Handbook*; Elsevier, 2005; ISBN 978−0123875822.
(34) Varrette, S.; Cartiaux, H.; Peter, S.; Kieffer, E.; Valette, T.; Olloh, A. *Proceeding of the 6th ACM High Performance Computing and Cluster Technologies Conference (HPCCT 2022)*; Fuzhou: China, 2022.Management of an Academic HPC & Research Computing Facility: The ULHPC Experience 2.0

https://doi.org/10.1021/acsomega.3c08862
ACS Omega 2024, 9, 10592−10601